An Organorhodium Anticancer Agent with a Non-conventional Mode of Action Based on a Histone Deacetylase Inhibitor and a Plectin-targeting Agent

Muhammad Hanif,*[a]1 Jahanzaib Arshad,[a]1 Jonathan W. Astin,[b] Zohaib Rana,[c] Ayesha Zafar,[a] Sanam Movassaghi,[a] Euphemia Leung,[c] Kamal Patel,[a] Tilo Söhnel,[a] Jóhannes Reynisson,[d] Vijayalekshmi Sarojini,[a] Rhonda J. Rosengren,[c] Stephen M. F. Jamieson,[e] Christian G. Hartinger*[a]

[a] Dr. M. Hanif, J. Arshad, A. Zafar, Dr. S. Movassaghi, K. Patel, Prof. T. Söhnel, Dr. V. Sarojini, Prof. C. G. Hartinger
School of Chemical Sciences
University of Auckland,
Private Bag 92019, Auckland 1142, New Zealand
E-mail: c.hartinger@auckland.ac.nz; m.hanif@auckland.ac.nz
web: http://hartinger.auckland.ac.nz/

[b] Dr. J. W. Astin
School of Medical Sciences
University of Auckland,
Private Bag 92019, Auckland 1142, New Zealand

[c] Zohaib Rana, Prof. Rhonda J. Rosengren
Department of Pharmacology and Toxicology
University of Otago,
Dunedin 9016, New Zealand

[d] Dr. J. Reynisson
School of Pharmacy and Bioengineering
Keele University
Staffordshire, ST5 5BG, United Kingdom

[e] Dr. E. Leung, Dr. S. M. F. Jamieson
Auckland Cancer Society Research Centre
University of Auckland
Private Bag 92019, Auckland 1142, New Zealand

[1] these authors contribute equally to the work.

Abstract: The combination of more than one pharmacophore in a mulitargeted anticancer agent may result in synergistic activity of its components. Using this concept, bioorganometallic compounds were designed to feature a metal center, a 2-pyridinecarbothioamide (PCA), and a hydroxamic acid, which is found in the anticancer drug vorinostat (SAHA). The organometallics showed inhibitory activity in the nanomolar range against histone deacetylases (HDACs) as the key target for SAHA. In particular, Rh complex **4c** was a potent inhibitor of HDAC6 over HDAC1 and HDAC8. While especially **4c** was highly cytotoxic in human cancer cells, it showed low toxicity in hemolysis studies and zebrafish, demonstrating the role of the metal center. The impact of the PCA moiety was established in the reduced expression of VEGFR2, which is upregulated by SAHA. This indicates that the new organometallics display different modes of action than its components, supporting the development of non-conventional anticancer drugs.

Histone deacetylases (HDACs) are overexpressed in solid tumor malignancies and in hematological cancers, leading to poor prognosis.[1] The upregulation of HDACs is known to induce tumor angiogenesis related to hypoxia.[2] The inhibition of HDACs using small molecules is an important therapeutic strategy in anticancer drug discovery, which has been validated by the FDA approval of vorinostat (suberoylanilide hydroxamic acid, SAHA)[3] and romidepsin (FK-228) for clinical use, both of which target the Zn^{II} ion of HDACs.[4] Moreover, modulation of the activity of HDACs can change the biological function of a diverse range of other proteins such as p53,[5] tubulin,[6] and Hsp90,[7] which are important therapeutic targets themselves. HDAC inhibitors (HDACi) have been shown to interfere with tumor angiogenesis,[2] and induce apoptosis in cancer stem cells.[8] HDACi have been suggested for cancer immunotherapy, due to their potent immunomodulatory activity both in tumour-bearing mice and cancer patients.[9]
Metal complexes with their tunable 3D shape offer a unique opportunity to develop compounds for selective recognition and interaction with the active sites of proteins.[10] Recently, there has been an increased interest in the design of metal complexes that target histones[11] or epigenetic enzymes.[12] Metal-based HDACi include compounds based on Pt,[13] $ReCp(CO)_3$,[14] ferrocene,[15] and Ru.[16]

In our efforts to design multitargeted anticancer agents, *i.e.* a drug contains more than one pharmacophore in a single molecule,[17] the design concept of the organometallic HDACi presented here is based on a bioactive metal center, that can undergo ligand exchange reactions and form covalent bonds to target donor atoms; a vorinostat-inspired hydroxamic acid moiety as the Zn-binding group; and a 2-pyridinecarbothioamide (PCA) ligand. PCA-based organometallics were

shown to interact selectively with plectin[18] and to have a preference for amino acid side chains over DNA, as shown in nucleosome core particle binding studies.[19] The high stability of PCA–metal bonds, even under acidic conditions, provides a structural scaffold suitable for oral administration.[19-20]

The PCA-based hydroxamic acid ligands **3** and **4** were prepared in two steps (Scheme 1). Succinic or suberic anhydride were reacted with *N*-(4-aminophenyl)pyridine-2-carbothioamide to afford PCA-succinic acid **1** and PCA-suberic acid **2** in yields of 61 and 41%, respectively. PCAs **1** and **2** were converted into the respective hydroxamic acids **3** (29%) and **4** (32%) with NH_2OH, ethylchloroformate, and Et_3N. This conversion was characterised by an upfield shift of the broad COOH singlet in the ^1H NMR spectra from *ca*. 12 ppm in **1** and **2** to *ca.* 8.70 ppm for the hydroxyl protons in **3** and **4**. X-ray diffraction analysis of a single crystal of **1** showed that it crystallized in the orthorhombic space group *Pbca* (Table S1, Figure S1). The C6=S1 bond length of 1.665(3) Å was significantly longer than found for the carbonyl groups C13=O1 and C15=O2 at 1.232(3) and 1.232(3) Å, respectively (Table S2). The aromatic rings are co-planar, stabilized by an intramolecular H bond between N1 of the pyridine ring and the amide H_{N2} (2.107 Å). The molecules form an expansive network of intermolecular H bonds that involve the carboxylic acid H_{O3} of one molecule and the carbonyl O2 of another ($H_{O3}\cdots$O2 distance of 2.669 Å; Figure S1). In addition, the amide proton H_{N3} and carbonyl oxygen form another set of intermolecular hydrogen bonds with an $H_{N3}\cdots$O1 distance of 2.085 Å.

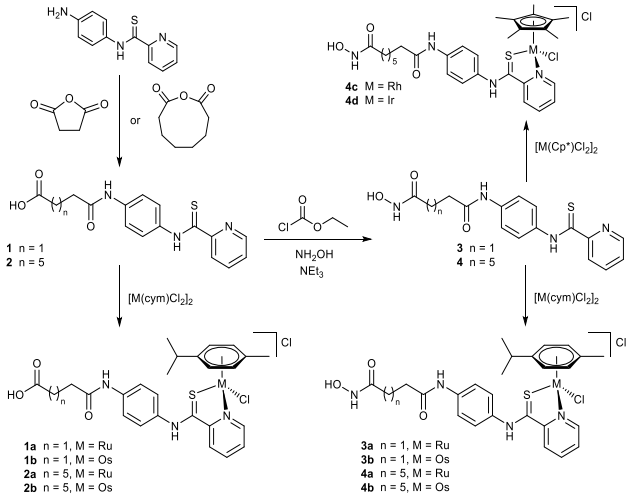

Scheme 1. Synthesis of the 2-pyridinecarbothioamide carboxylic (**1** and **2**) and hydroxamic acids (**3** and **4**) and their respective organometallic Ru^{II} (**a**), Os^{II} (**b**), Rh^{III} (**c**) and Ir^{III} (**d**) complexes.

Both the carboxylic (**1** and **2**) and hydroxamic (**3** and **4**) acid derivatives were converted to organometallics by reaction with the dimeric precursors $[M(cym)Cl_2]_2$ (M = Ru, Os; cym = η^6-*p*-cymene) or $[M(Cp^*)Cl_2]_2$ (M = Rh, Ir; Cp* = pentamethylcyclopentadienyl) in 37–75% yield. In the ^1H NMR spectra, coordination of **1**–**4** to the metal ions caused deshielding of the pyridine proton H1 accompanied by downfield shifts of *ca.* 1 ppm depending on the metal center (δ = 9.1–9.7 ppm). In contrast, H4, which is involved in a hydrogen bond with S1 in the crystal structure of **1**, becomes more shielded and shifts upfield by *ca.* 0.2 ppm to around 8.5 ppm. $^{13}C\{^1H\}$ NMR spectroscopy confirmed the structural characterization, although not all of the C atoms were detectable. The compounds were also characterized by elemental analysis and electrospray ionization mass spectrometry (ESI-MS), all of which supported the identity of the compounds. The ESI-mass spectra of all complexes featured $[M - 2Cl - H]^+$ ions as base peaks with the experimental *m/z* values and isotope distributions in close agreement to the calculated values. This shows the ease of deprotonation of the thioamide proton while in the solid state the amide remains protonated. This was confirmed by single crystal X-ray diffraction analysis of **1b** (Table S1). Complex **1b** crystallized in the monoclinic space group $P2_1/c$ as two enantiomers and the structure featured the characteristic piano-stool configuration where the Os is coordinated to cym, the *S,N*-chelating PCA **1**, and a chlorido ligand (Figure 1). The chloride counterion formed intermolecular H bonds with the amide proton H_{N3} and the thioamide proton H_{N2} to bridge two enantiomeric molecules of **1b** (Figure S2). The Os−$cym_{centroid}$ and the Os–Cl distances of 1.679(1) Å and 2.417(2) Å, respectively, were in a similar range as observed for structurally related [Os(cym)(PCA)Cl] complexes.[19] For coordination of the Os centre to S1 and N1, the H bond N1$\cdots H_{N2}$ for in **1** was broken. This resulted in the PCA ligand to lose its planarity (torsion angle C5–C6–N2–C7 135.08°) seen in the molecular structure of **1**. Upon metal coordination, the bond C6–S1 was elongated (1.691(6) Å vs. 1.665(3) Å), as observed for related compounds.[19-20] This indicates higher single bond character for C6–S1 and higher double bond character for the C6–N2 bond.

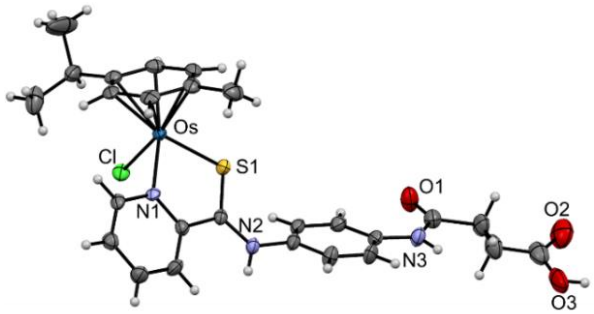

Figure 1. Molecular structure of one of the enantiomers of **1b** drawn at 50% probability level. The counter ion and residual MeOH were removed for clarity.

The stability of **4a**–**4d** in D_4-MeOD/D_2O (**4a** and **4b**) or D_2O (**4c** and **4d**) was studied by ^{1}H NMR spectroscopy (Figures S3 and S4). Compound **4c** was remarkably soluble in water (47 mM), especially compared to **4d** (0.6 mM). All complexes underwent chlorido/aqua ligand exchange, which was complete within 15 min for **4a**, **4c** and **4d** and too fast to determine reaction kinetics for by NMR spectroscopy, while **4b** reacted more slowly and the process took about 6 h. The formation of the aqua complexes was confirmed by addition of 2 eq. of $AgNO_3$, which gave identical spectra (Figure S3). The aqua species were stable for at least 5 d. The ligand exchange appeared to be at least partly reversible in the presence of 104 mM NaCl or 60 mM HCl, however, precipitation of probably the chlorido complex complicated data interpretation. The reversibility of the ligand exchange reaction was indicated, for example, in the case of **4c** by a shift of the signal assigned to H1 from 8.41 ppm for the aqua species to 9.08 ppm for the chlorido complex in the ^{1}H NMR spectra (Figure S3).
Furthermore, **4a**–**4d** were studied for their reactions with L-cysteine (Cys), L-methionine (Met), L-histidine (His), in 5% D_4-MeOD/D_2O (**4a** and **4b**) or D_2O (**4c** and **4d**) by ^{1}H NMR spectroscopy (Figure S5). These experiments supported the results found in the stability studies. The compounds were highly stable and no adduct formation with His, Met or Cys was observed over 5 d. This level of stability of the compounds is remarkable, especially in presence of Cys, which has been reported to induce decomposition of Ru(arene) complexes.[19]
The cytotoxicity of the PCAs **1**–**4** and their organometallic complexes was determined by the SRB assay in human colorectal (HCT116), non-small cell lung (H460), cervical (SiHa) and colon carcinoma (SW480) cells (Tables 1 and S3). Of the carboxylic acid derivatives and their complexes, only PCA **2** was moderately cytotoxic while for none of the complexes of **1** and **2** an IC_{50} value could be reached in the concentration range investigated. The hydroxamic acid derivatives **3** and **4** showed antiproliferative activity, especially the SAHA analogue **4**, which gave IC_{50} values in the high nanomolar range (Table 1) and was at least 2 orders of magnitude more potent than its carboxylic acid derivative **2**. This demonstrates the essential role of the hydroxamic acid functional group in the biological activity of many HDACi. Only the organometallic compounds formed with **4** showed cytotoxicity and their potency depended strongly on the metal fragment. Ru(cym) **4a** and Os(cym) **4b** were low to moderately cytotoxic, while the Cp* complexes of Rh **4c** and Ir **4d** showed the highest antiproliferative activity, with **4c** being similarly cytotoxic as **4**. To evaluate whether the redox chemistry of the metal center was the source of the difference in activity of **4a** and **4c** (Ru vs Rh), their ability to induce the formation of reactive oxygen species (ROS) was investigated but neither of the compounds showed higher ROS generation than the untreated control.

Table 1. *In vitro* cytotoxic activity (mean IC_{50} values ± standard deviations) of PCA-hydroxamic acid **4** and its organometallic complexes **4a**–**4d** in the human cancer cell lines HCT116 (colon), NCI-H460 (non-small cell lung), SiHa (cervix), and SW480 (colon) given in µM as determined by the SRB assay (exposure time 72 h)**.**

compound	**IC_{50} values (µM)**			
	HCT116	NCI-H460	SiHa	SW480
SAHA	0.46 ± 0.09	0.57 ± 0.01	1.6 ± 0.1	1.3 ± 0.07
4	0.30 ± 0.14	0.98 ± 0.30	1.6 ± 0.6	1.5 ± 0.3
4a	30 ± 3	120 ± 24	126 ± 15	124 ± 8
4b	42 ± 5	136 ± 71	73 ± 5	170 ± 124
4c	0.97 ± 0.10	3.5 ± 0.3	3.3 ± 0.1	3.3 ± 0.2
4d	3.4 ± 0.5	11.4 ± 0.6	12 ± 0.3	11 ± 1

Based on the cytotoxic data, **2**–**4** and **4a**–**4d** were selected for screening of HDAC8 inhibition at a concentration of 10 µM. The carboxylic acid **2** and the hydroxamic acid **3** showed very low activity at this concentration with residual HDAC8 activity of 100 and 83%, respectively (Table S4). The presence of the hydroxamic acid in **3** proved beneficial with a slight inhibition of HDAC8 and this was confirmed for the SAHA derivative **4** with only 9% residual HDAC8 activity. This fact demonstrates the role of the length of the aliphatic chain which is required for the hydroxamic acid group to reach the Zn ion deep in the active site of the enzyme. Notably, all complexes of **4** were more potent than the ligand at this concentration

and they were therefore included in a study to determine their IC_{50} values against HDAC1, HDAC6 and HDAC8 (Table 2). PCA **4** and its organometallic compounds **4a**–**4d** exhibited excellent HDAC inhibitory potential with IC_{50} values in the nM range, with coordination to organometallic moieties enhancing the HDAC1 and HDAC8 inhibitory activity of **4**. The complexes were up to 10-fold more potent inhibitors of HDAC1 and HDAC8 than the clinically approved drug SAHA, while **4** and its Rh(Cp*) complex **4c** were 3-4 fold more potent inhibitors of HDAC6 compared to SAHA. In general, the organometallic compounds showed a slight selectivity for HDAC6, as would be expected given their structural similarity with SAHA, which was about an order of magnitude more potent against HDAC6 than HDAC1 and HDAC8 in this assay. The influence of the metal center may be explained by two effects. It can undergo ligand exchange reactions and despite not seeing adduct formation with isolated amino acids, the protein microenviroment may support interaction within the binding site of HDACs.[19] Moreover, the metal fragment can be considered as a bulky group that may form hydrophobic interactions or hydrogen bonds with aromatic amino acid side chains.[21] Comparison of the HDAC inhibitory and cytotoxicity data shows some correlation for HDAC6. In addition, the PCA ligand and the metal center may contribute to the biological activity through alternative pathways.

Table 2. Inhibitory activity (IC_{50} in nM) of PCA-hydroxamic acid **4** and its organometallic complexes **4a–4d** against HDAC1, HDAC6, and HDAC8 in comparison to SAHA.

compound	**IC_{50} values (nM)**		
	HDAC1	HDAC6	HDAC8
SAHA	301 ± 21	16 ± 1.5	840 ± 24
4	458 ± 22	4 ± 1.5	759 ± 201
4a	44 ± 24	15 ± 0.5	53 ± 11
4b	45 ± 16	32 ± 11	99 ± 16
4c	173 ± 30	5 ± 1	29 ± 6
4d	67 ± 18	11 ± 0.6	29 ± 3

The acetylation/deacetylation of histone proteins allows for the regulation of transcription. Removal of acetyl groups from histones by HDACs results in the suppression of transcription. SAHA is a potent HDAC inhibitor, in particular of HDAC6 (Table 2), and was compared with the most active compounds **4** and **4c** in terms of its potency to inhibit histone H3 deacetylation in prostate carcinoma (PC3) cells (Figure 2) at concentrations of 1, 2 and 4 µM. Analysis of the immunblotting data for acetyl-H3 relative to β-tubulin suggests a concentration-dependent inhibitory potency for all three compounds, compared to the negative control, although only the data for SAHA was found to be statistically significant. SAHA was overall slightly more potent than **4** and **4c**.

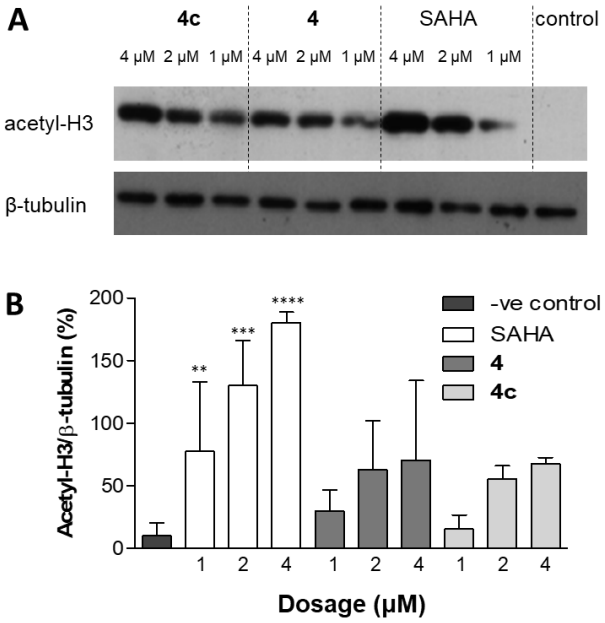

Figure 2. Acetylation of histone variant H3 has been shown in response to SAHA, **4** and **4c** at concentrations of 1, 2 and 4 µM in the PC3 cell line (n = 3). (A) Blot highlighting the differences in acetylation between different drugs, and (B) densitometry was used to quantify blots; **, *** and **** indicate p-values of <0.01, <0.001 and <0.0001.

To understand the HDAC inhibitory activity of **4** and the two enantiomers of its complexes **4a**–**4d** in comparison to SAHA, a molecular modelling approach was used in combination with molecular dynamics simulations. The active site of HDAC8

consists of a long, narrow channel leading to a cavity that contains the catalytic machinery. The walls of the channel are formed by Tyr100, Tyr306, His180, Phe152, Gly151 and Met 274 and are primarily hydrophobic.[22] Studies with SAHA confirmed that the Zn^{2+} ion and also Tyr306 are the important active site components (Table S5).[15a, 22b] Upon modelling, **4** and its enantiomeric metal complexes showed a good fit in the binding pocket as they superimposed SAHA and interacted with Zn through the hydroxamate motif (Figure S6 for **4b^{E2}**). In all cases, the metal fragments were sitting above the protein surface. With the exception of one of the enantiomers of **4c**, the complexes formed H bonds with His180 (and the majority also with Asp101), while all but one of the enantiomers of **4b** and **4** showed lipophilic contacts with Tyr100 through the ligand backbone (Table S5). The latter fact may be of relevance when interpreting the HDAC inhibition data for **4** which was by far the least active HDAC8 inhibitor.

Modelling the same compounds into HDAC6 resulted in similar observations as for HDAC8 with the compounds interacting with the Zn ion but the metal complexes were found lying in a nearby second channel as compared with SAHA and **4**. This positioning supports additional interactions of the metal moiety with the protein through functionally important active site residues such as Tyr745, Pro464, Phe583, His463 and Gly473 (Figure 3 for **4c^{E2}**, Table S6).[23] Notably, the enantiomeric structures offer different binding options with amino acid side chains, most significantly His463 with its imidazole moiety, which may well undergo a ligand exchange reaction with one enantiomer, while the other has the labile chlorido ligand pointing away from it.

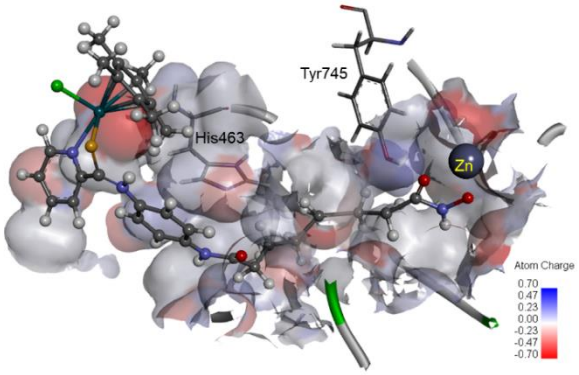

Figure 3. The modelled configuration of **4c^{E2}** in the binding site of HDAC6 (PDB ID 5eei). The complex is shown in the binding pocket with the protein surface rendered. Blue depicts a positive partial charge on the surface, red negative and grey neutral/lipophilic.

The hemolytic activity of the most potent **4c** to mouse red blood cells was assessed to gain further insight into its toxicity. At low concentrations similar to the IC_{50} values, **4c** was not hemolytic. When the concentration was increased to 200 µM, **4c** showed about 10% hemolytic activity which was significantly lower toxicity than for example found for cisplatin which displays 100% hemolytic activity at this concentration.[24]

The prognosis for patients with solid tumors is known to be angiogenesis-dependent.[25] HDACs, among many cellular functions, are closely linked to tumor angiogenesis, in particular under hypoxic environment.[2a] In pre-clinical animal models and clinical studies, the HDAC inhibitors SAHA and panobinostat have shown promising antiangiogenic activity.[26] Therefore, **4**, **4c** and for comparison SAHA were evaluated for their *in vivo* antiangiogenic activity in transgenic zebrafish at concentrations of 2 µM. Notably, the treatment of the zebrafish embryos with the Rh compound **4c** substantially reduced the formation of new blood vessels in comparison to **4** and clinically used HDAC inhibitor SAHA (Figure 4).

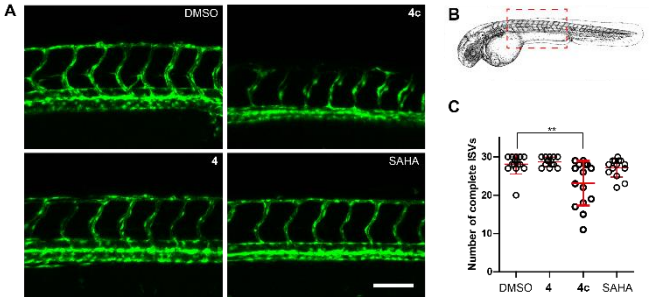

Figure 4. Confocal images of the developing trunk vasculature in 48 hpf (hours post fertilization) in *fli1a:EGFP* zebrafish embryos treated with either vehicle (DMSO) or 2 µM of either SAHA, **4** or **4c**. (**B**) Schematic of a 48 hpf embryo showing the location of confocal images. (**C**) Quantitation of intersegmental vessel (ISV) formation at 48 hpf in treated embryos (n > 14 for all treatment groups). Embryos treated with **4c** have impaired vascular development compared to the control. Scale bar = 100 µm. ** p<0.005 by Mann-Whitney test.

Compounds **4** and **4c** were evaluated for protein expression levels of vascular endothelial growth factor receptor 2 (VEGFR2) and vascular endothelial growth factor A (VEGFA) in prostate carcinoma (PC3) cells using Western blotting. VEGFA is a cytokine that binds to VEGFR2, a tyrosine kinase receptor.[27] An insight into the regulation of these markers can provide information about the downstream pathways including protein kinase B (AKT), focal adhesion kinase (FAK) and proto-oncogene tyrosine-protein kinase (SRC) that in turn stimulate angiogenesis.[28] At all concentrations investigated, both **4** and **4c** significantly reduced the expression of VEGFR2 as compared to the negative control after treatment for 24 h, while SAHA was shown to upregulate VEGFR2 at the same concentrations (Figure 5). This indicates a significant impact of the PCA moiety while there was hardly any difference between the PCA-derived ligand and its Rh complex.

Both compounds showed slightly higher reductions in VEGFA compared to SAHA, however, without being statistically significant relative to the negative control (Figure S7). SAHA has been shown to induce sprouting of endothelial cell spheroids albeit at a higher concentration of 5 mM.[29] Reasons for this can be attributed to the differential effects of HDACs in different environments,[27b, 27c] and also HDACs can effect multiple gene expressions.

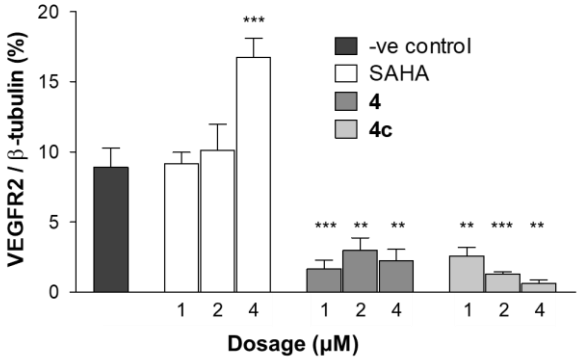

Figure 5. VEGFR2 expression assessed as a percentage of β-tubulin in PC3 cells using Western blotting after 24 h. Data was quantified using densitometry. Concentrations of 1, 2 and 4 μM of **4** and **4c** were compared with SAHA. Mean ± SEM was plotted for each of the treatments; *, ** and *** indicate p-values of <0.05, <0.01 and <0.001, respectively compared to -ve control and was determined using parametric variant of Anova and multiple Tukey's test (n = 3).

In conclusion, we report an approach of combining different pharmacophores in a single molecule in an attempt to design potent anticancer agents targeting HDACs. To elucidate the role of each component of the target molecules, the bioactive PCA moiety was functionalized with hydroxamic and carboxylic acid residues and both the linker and metal fragment were varied. This led to the identification of PCA **4**, which is structurally related to SAHA, and its Rh complex **4c** as the most potent cytotoxins. While **4c** was found to be highly cytotoxic, no hemolytic activity in mouse red blood cells was detected. Ligand **4** and its metal complexes showed a similar HDACi pattern as SAHA in HDAC1, HDAC6 and HDAC8 inhibition studies, which correlated to some extent with the cytotoxic activity but also suggested an impact of the other bioactive moieties beyond the SAHA-derived fragment on the biological activity. Zebrafish experiments suggested anti-angiogenic activity of the Rh complex **4c** over that of **4**, demonstrating the impact of the metal center. The reduction of VEGFR2 expression supports this observation from the *in vivo* studies. This demonstrates that careful selection of bioactive moieties resulted in enhanced biological activity where each component of a single molecule has a special role to play in the search for new compounds with non-classical modes of action.

Acknowledgements

We thank the University of Auckland for financial support. The authors are grateful to Tanya Groutso for collecting the X-ray crystal data, Tony Chen for ESI-MS analyses and Stuart Morrow for help with the ICP-MS measurements.

Keywords: Anticancer agents • Bioorganometallics • HDAC inhibitors • Antiangiogensis • Metal arene

[1] a) R. W. Johnstone, *Nat. Rev. Drug Discovery* **2002**, *1*, 287-299; b) C. B. Yoo, P. A. Jones, *Nat. Rev. Drug Discovery* **2006**, *5*, 37-50; c) S. G. Royce, K. Ververis, T. C. Karagiannis, *Ann. Clin. Lab. Sci.* **2012**, *42*, 338-345; d) K. J. Falkenberg, R. W. Johnstone, *Nat. Rev. Drug Discovery* **2014**, *13*, 673-691.

[2] a) L. Ellis, H. Hammers, R. Pili, *Cancer Letters* **2009**, *280*, 145-153; b) M. New, H. Olzscha, N. B. La Thangue, *Mol Oncol* **2012**, *6*, 637-656; c) I. Hrgovic, M. Doll, A. Pinter, R. Kaufmann, S. Kippenberger, M. Meissner, *Exp Dermatol* **2017**, *26*, 194-201.

[3] B. S. Mann, J. R. Johnson, M. H. Cohen, R. Justice, R. Pazdur, *Oncologist* **2007**, *12*, 1247-1252.

[4] C. Grant, F. Rahman, R. Piekarz, C. Peer, R. Frye, R. W. Robey, E. R. Gardner, W. D. Figg, S. E. Batest, *Expert Rev. Anticancer Ther.* **2010**, *10*, 997-1008.

[5] W. Gu, R. G. Roeder, *Cell* **1997**, *90*, 595-606.

[6] C. Hubbert, A. Guardiola, R. Shao, Y. Kawaguchi, A. Ito, A. Nixon, M. Yoshida, X. F. Wang, T. P. Yao, *Nature* **2002**, *417*, 455-458.
[7] J. J. Kovacs, P. J. M. Murphy, S. Gaillard, X. A. Zhao, J. T. Wu, C. V. Nicchitta, M. Yoshida, D. O. Toft, W. B. Pratt, T. P. Yao, *Mol Cell* **2005**, *18*, 601-607.
[8] M. Dvorakova, T. Vanek, *MedChemComm* **2016**, *7*, 2217-2231.
[9] L. Shen, A. Orillion, R. Pili, *Epigenomics* **2016**, *8*, 415-428.
[10] a) M. S. Finnin, J. R. Donigian, A. Cohen, V. M. Richon, R. A. Rifkind, P. A. Marks, R. Breslow, N. P. Pavletich, *Nature* **1999**, *401*; b) K. V. Butler, J. Kalin, C. Brochier, G. Vistoli, B. Langley, A. P. Kozikowski, *Journal of the American Chemical Society* **2010**, *132*, 10842-10846.
[11] B. S. Murray, M. V. Babak, C. G. Hartinger, P. J. Dyson, *Coord. Chem. Rev.* **2016**, *306*, 86-114.
[12] C. H. Leung, L. J. Liu, K. H. Leung, D. L. Ma, *Coord. Chem. Rev.* **2016**, *319*, 25-34.
[13] a) D. Griffith, M. P. Morgan, C. J. Marmion, *Chem. Commun.* **2009**, 6735-6737; b) V. Brabec, D. M. Griffith, A. Kisova, H. Kostrhunova, L. Zerzankova, C. J. Marmion, J. Kasparkova, *Mol. Pharmaceutics* **2012**, *9*, 1990-1999.
[14] D. Can, H. W. Peindy N'Dongo, B. Spingler, P. Schmutz, P. Raposinho, I. Santos, R. Alberto, *Chem. Biodiversity* **2012**, *9*, 1849-1866.
[15] a) J. Spencer, J. Amin, R. Boddiboyena, G. Packham, B. E. Cavell, S. S. Syed Alwi, R. M. Paranal, T. D. Heightman, M. Wang, B. Marsden, P. Coxhead, M. Guille, G. J. Tizzard, S. J. Coles, J. E. Bradner, *MedChemComm* **2012**, *3*, 61-64; b) J. de Jesús Cázares-Marinero, S. Top, A. Vessières, G. Jaouen, *Dalton Trans.* **2014**, *43*, 817-830.
[16] R.-R. Ye, Z.-F. Ke, C.-P. Tan, L. He, L.-N. Ji, Z.-W. Mao, *Chem. Eur. J.* **2013**, *19*, 10160-10169.
[17] E. Petruzzella, J. P. Braude, J. R. Aldrich-Wright, V. Gandin, D. Gibson, *Angew. Chem., Int. Ed. Engl.* **2017**, *56*, 11539-11544.
[18] S. M. Meier, D. Kreutz, L. Winter, M. H. M. Klose, K. Cseh, T. Weiss, A. Bileck, B. Alte, J. C. Mader, S. Jana, A. Chatterjee, A. Bhattacharyya, M. Hejl, M. A. Jakupec, P. Heffeter, W. Berger, C. G. Hartinger, B. K. Keppler, G. Wiche, C. Gerner, *Angew. Chem., Int. Ed. Engl.* **2017**, *56*, 8267-8271.
[19] S. M. Meier, M. Hanif, Z. Adhireksan, V. Pichler, M. Novak, E. Jirkovsky, M. A. Jakupec, V. B. Arion, C. A. Davey, B. K. Keppler, C. G. Hartinger, *Chem. Sci.* **2013**, *4*, 1837-1846.
[20] J. Arshad, M. Hanif, S. Movassaghi, M. Kubanik, A. Waseem, T. Söhnel, S. M. F. Jamieson, C. G. Hartinger, *J. Inorg. Biochem.* **2017**, *177*, 395-401.
[21] M. P. Sullivan, M. Groessl, S. M. Meier, R. L. Kingston, D. C. Goldstone, C. G. Hartinger, *Chem. Commun.* **2017**, *53*, 4246-4249.
[22] a) J. R. Somoza, R. J. Skene, B. A. Katz, C. Mol, J. D. Ho, A. J. Jennings, C. Luong, A. Arvai, J. J. Buggy, E. Chi, *Structure* **2004**, *12*, 1325-1334; b) T. Sundarapandian, J. Shalini, S. Sugunadevi, L. K. Woo, *J. Mol. Graphics Modell.* **2010**, *29*, 382-395.
[23] Y. Hai, D. W. Christianson, *Nat. Chem. Biol.* **2016**, *12*, 741.
[24] S. Parveen, M. Hanif, E. Leung, K. K. H. Tong, A. Yang, J. Astin, G. H. De Zoysa, T. R. Steel, D. Goodman, S. Movassaghi, T. Söhnel, V. Sarojini, S. M. F. Jamieson, C. G. Hartinger, *Chem. Commun.* **2019**, *55*, 12016-12019.
[25] J. Hasan, R. Byers, G. C. Jayson, *Br. J. Cancer* **2002**, *86*, 1566-1577.
[26] a) L. Ellis, Y. Pan, G. K. Smyth, D. J. George, C. McCormack, R. Williams-Truax, M. Mita, J. Beck, H. Burris, G. Ryan, P. Atadja, D. Butterfoss, M. Dugan, K. Culver, R. W. Johnstone, H. M. Prince, *Clin. Cancer Res.* **2008**, *14*, 4500-4510; b) M. Duvic, R. Talpur, X. Ni, C. L. Zhang, P. Hazarika, C. Kelly, J. H. Chiao, J. F. Reilly, J. L. Ricker, V. M. Richon, S. R. Frankel, *Blood* **2007**, *109*, 31-39.
[27] a) M. Kim, K. Jang, P. Miller, M. Picon-Ruiz, T. M. Yeasky, D. El-Ashry, J. M. Slingerland, *Oncogene* **2017**, *36*, 5199-5211; b) C. Urbich, L. Rossig, D. Kaluza, M. Potente, J. N. Boeckel, A. Knau, F. Diehl, J. G. Geng, W. K. Hofmann, A. M. Zeiher, S. Dimmeler, *Blood* **2009**, *113*, 5669-5679; c) A. Turtoi, D. Mottet, N. Matheus, B. Dumont, P. Peixoto, V. Hennequiere, C. Deroanne, A. Colige, E. De Pauw, A. Bellahcene, V. Castronovo, *Angiogenesis* **2012**, *15*, 543-554.
[28] T. T. Huang, Y. W. Lan, Y. F. Ko, C. M. Chen, H. C. Lai, D. M. Ojcius, J. Martel, J. D. Young, K. Y. Chong, *J Ethnopharmacol* **2018**, *220*, 239-249.
[29] G. Jin, D. Bausch, T. Knightly, Z. C. Liu, Y. Q. Li, B. L. Liu, J. Lu, W. Chong, G. C. Velmahos, H. B. Alam, *Surgery* **2011**, *150*, 429-435.